Morphology and interdiffusion behavior of evaporated metal films on crystalline diindenoperylene thin films

A. C. Dürr[a)]
Max-Planck-Institut für Metallforschung, Heisenbergstrasse 3, 70569 Stuttgart, Germany

F. Schreiber[b)]
Max-Planck-Institut für Metallforschung, Heisenbergstrasse 3, 70569 Stuttgart, Germany and Universität Stuttgart, Pfaffenwaldring 57, 70550 Stuttgart, Germany

M. Kelsch
Max-Planck-Institut für Metallforschung, Heisenbergstrasse 3, 70569 Stuttgart, Germany

H. D. Carstanjen and H. Dosch
Max-Planck-Institut für Metallforschung, Heisenbergstrasse 3, 70569 Stuttgart, Germany and Universität Stuttgart, Pfaffenwaldring 57, 70550 Stuttgart, Germany

O. H. Seeck
IFF, FZ Jülich GmbH, 52425 Jülich, Germany and Hasylab at DESY, Notkestrasse 85, 22603 Hamburg, Germany

(Received 23 October 2002; accepted 7 January 2003)

We present a transmission electron microscopy (TEM)/Rutherford backscattering spectrometry (RBS)/x-ray-diffraction (XRD) study of Au evaporated on crystalline organic thin films of diindenoperylene (DIP). Cross-sectional TEM shows that the preparation conditions of the Au film (evaporation rate and substrate temperature) strongly determine the interfacial morphology. *In situ* XRD during annealing reveals that the organic layer is thermally stable up to about 150 °C, a temperature sufficient for most electronic applications. The x-ray measurements show that the ''as-grown'' Au layer exhibits a large mosaicity of around 10°. Upon annealing above ≈120 °C the Au film starts to reorder and shows sharp (111)-diffraction features. In addition, temperature-dependent RBS measurements indicate that the Au/DIP interface is thermally essentially stable against diffusion of Au in the DIP layer up to ≈100 °C on the time scale of hours, dependent on the Au thickness. © *2003 American Institute of Physics.* [DOI: 10.1063/1.1556180]

I. INTRODUCTION

Due to their exciting electronic, optical, and optoelectronic properties, organic semiconductors have experienced a tremendous increase in research activities over the last few years. Several organic electronic devices have been demonstrated, such as full-color, large-area, organic light-emitting diode displays,[1–4] flexible photovoltaic cells,[5,6] organic field-effect transistors with high on/off ratio,[7–9] and examples of physical as well as chemical organic thin film sensors.[10] All these devices operate with one or several functional organic layers with the desired physical properties and metal–organic contacts to inject (or extract) charge carriers. In several device geometries, these metal contacts are deposited on top of the organic film. The proper function of the contact is prerequisite for the performance of the device, and it depends on the interfacial morphology of the metal–organic interface. An important issue for technical applications is also the thermal stability of the organic layer itself as well as that of the metal-organic interface, since the devices may be exposed to elevated temperatures during the fabrication process (e.g., soldering) or during operation (e.g., due to Ohmic losses).

Until now, these structural issues have been addressed by only a limited number of studies carried out mostly on disordered polymers which are used as low dielectric constant material in conventional microelectronic fabrication processes;[11–16] in addition, some studies have been published on Langmuir–Blodgett films[17] and on organic thin films deposited under ultra-high-vacuum (UHV) conditions.[18–22] The thermal stability of solution-grown systems with organic–inorganic interfaces was studied in Ref. 23.

In this work, Au deposited under various conditions on diindenoperylene thin films [$C_{32}H_{16}$, diindenoperylene (DIP), see Fig. 1] is studied as a model system for metal contacts on organic electronic devices (a short report of some aspects of this work has previously been published in Ref. 22). DIP has been chosen as the organic material, since it forms closed films with high structural order, if deposited under suitable conditions on silicon dioxide.[24] Furthermore, these DIP films show a charge carrier (hole) mobility μ_h up to 0.1 cm^2/V s at room temperature.[25] Au is widely used as a hole-injecting metal.

To understand how the metal–organic interface morphology depends on the conditions employed during deposition of the metal layer, the main processes involved in

a)Author to whom correspondence should be addressed; electronic mail: Arndt.Duerr@mf.mpg.de
b)Now at: Physical and Theoretical Chemistry Laboratory, University of Oxford, South Parks Road, Oxford OX1 3QZ, United Kingdom.

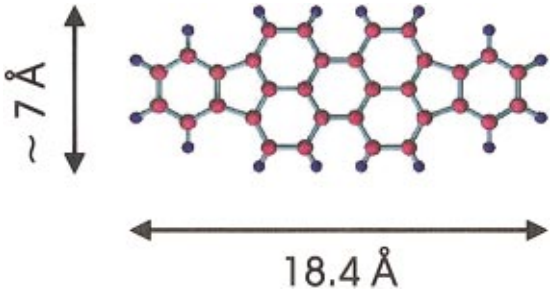

FIG. 1. (Color) Structure of a DIP molecule.

interface-formation are sketched qualitatively in the following: Upon arrival on the surface the metal atoms can either stick on the surface, diffuse along the surface with a certain diffusion constant $D_{\parallel}$ or penetrate the surface with a diffusion constant $D_{\perp}$ (presumably, $\ll D_{\parallel}$).[16,26,27] If a metal atom meets other metal atom(s) they form a cluster, the diffusion constants of which are expected to be strongly reduced so that even small clusters may be considered as ''immobile.''

Based on this simple model, three main parameters are identified that determine the morphology of the interface between the metal contact and the organic thin film.

(a) The substrate temperature during metal deposition: Lower temperatures lead to less mobile metal atoms, thus, less diffusion into the organic layer is expected.
(b) The deposition rate of the metal: The larger the deposition rate the larger is the probability for a metal atom at the surface to be met by freshly deposited atoms and form an immobile cluster before penetrating the surface. Note, however, that extremely high deposition rates (exceeding ≈ 10 Å/s) may deteriorate the organic surface.
(c) The interaction between the metal and the organic molecules: Metals that interact more strongly on the organic film may exhibit less interdiffusion into the organic film.

II. EXPERIMENT

Au films were prepared on DIP films under four different deposition conditions employing all combinations of low and high substrate temperature (-120 and $+70$ °C) with low and high deposition rates (0.35 and 23 Å/min); see Table I.

These samples (A1–A4) were examined by cross-sectional transmission electron microscopy (TEM) and by temperature-dependent x-ray scattering studies.

TABLE I. Preparation conditions of the Au layer on top of the DIP film.

Sample	T_{sub} °C	Rate Å/min	Nominal thickness Å	Analyzed by
A1	−120	23	120	TEM/x-rays
A2	−120	0.35	120	TEM/x-rays
A3	+70	23	135	TEM/x-rays
A4	+70	0.35	135	TEM/x-rays
A5	+25	1	35	RBS

All samples were prepared on smooth oxidized (4000 Å) Si(100) substrates. A DIP layer of typically 400 Å in thickness was grown at a substrate temperature of 145 ± 5 °C and at a rate of (12 ± 3) Å/min under UHV conditions leading to films of high structural order with a surface roughness of $\sigma \approx 25$ Å (≈ 1.5 ML DIP).[24,28] The Au film was deposited after growth of the DIP film in the same chamber.

TEM micrographs were taken with a JEOL FX4000 and with a Philips CM200 microscope at 400 and 200 kV, respectively. A detailed description of the preparation of the TEM-samples can be found in Ref. 29.

The Rutherford backscattering spectrometry (RBS) data were taken at the Stuttgart Pelletron[30] with He^+ ions at 1.3 MeV and a scattering angle of $\theta = 75°$. A high energy resolution spectrometer[31] was used with an energy resolution of $\Delta E = 2.4$ keV, corresponding to a depth resolution of ≈ 10 Å in Au.

For the temperature-dependent measurements, the samples were mounted on a heater in vacuum, annealed at a given temperature for 1 h,[32] and measured *in situ* using x-ray reflectivity and RBS, respectively, at each temperature step.

X-ray measurements were carried out at beamline W1 at HASYLAB in Hamburg, Germany, with an x-ray wavelength of $\lambda = 1.39$ Å. Figure 2 sketches the x-ray scattering geometry in real and reciprocal space, respectively. Three different types of scans were taken.

(1)The ''specular diffraction mode,'' where the incident angle α_i equals the exit angle α_f. Thus, the momentum transfer is normal to the surface [$\mathbf{q} = (0,0,q_z)$] and the electron density profile along z is probed. Within semikinematic scattering theory, the specularly scattered intensity is given by[33]

$$I(q_z) \propto R_F(q_z) \left| \frac{1}{\rho_{\mathrm{el},\infty}} \int_{-\infty}^{\infty} \frac{d\rho_{\mathrm{el}}(z)}{dz} \; e^{iq_z z} dz \right|^2, \qquad (1)$$

where $R_F(q_z)$ is the Fresnel reflectivity of the substrate, $d\rho_{\mathrm{el}}(z)/dz$ is the derivative of the electron density of the sample with respect to z, $\rho_{\mathrm{el},\infty}$ the electron density of the substrate.

In a layered system, the interference of x rays scattered at the different interfaces within the sample gives rise to intensity oscillations for small momentum transfer $\mathbf{q}$ (''Kiessig fringes''). The periodicity of these fringes $\Delta q_{K,z}$ is related to the thickness of a layer, D, by $D \approx 2\pi/\Delta q_{K,z}$ [e.g., D_{DIP} and D_{Au}; see Figs. 5(a) and 6(a)]. Interfacial roughness (σ) gives rise to a damping factor $\exp(-\sigma^2 q_z^2)$.

For larger q_z, the interference of individual atomic/molecular monolayers with lattice constant d within a given layer gives rise to Bragg reflections at the positions $q_z = 2\pi/d$. The integrated intensity of a Bragg reflection is related to the total number of coherent scatterers, N^*[34] [e.g., the gray shaded area in Figs. 5(a) and 6(a) is related to N^*_{DIP}].

If the layer consists of ordered (i.e., coherently scattering) domains which exhibit a homogeneous thickness D^*, satellite peaks, the so-called Laue oscillations appear near the main Bragg reflection, with a scattering amplitude given by

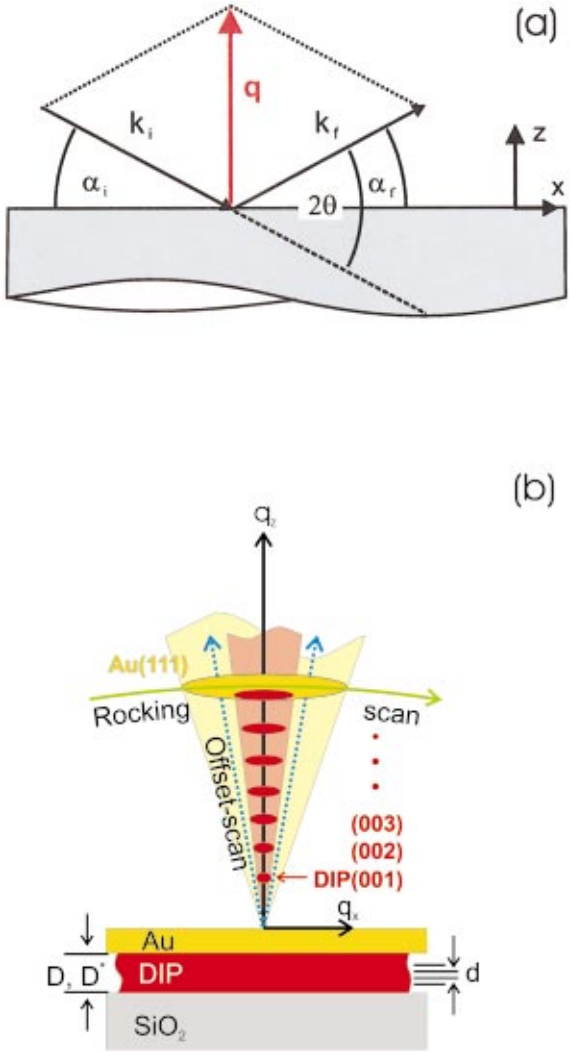

FIG. 2. (Color) (a) Geometry and symbols used in the text to describe different scan geometries in real space. $\mathbf{k_i}$ and $\mathbf{k_f}$ are the wave vectors of the incident and of the exit x-ray wave, while α_i and α_f denote the incident and the exit angle of these waves, respectively. $\mathbf{q}=\mathbf{k_f}-\mathbf{k_i}$ is the momentum transfer inside the sample. $2\Theta=\alpha_i+\alpha_f$ is the scattering angle. (b) Schematic of the three different scan modes in reciprocal space. The filled ellipses denote the location of the first seven specular DIP Bragg reflections and of the specular Au(111) Bragg reflection, respectively. The extension of the Bragg reflections in q_x direction represents the mosaicity of the related layer. The shaded triangular areas indicate the regions where specularly reflected intensity of DIP (narrow red triangle) and of Au (broad yellow triangle) is measured. D and D^* denote the film thickness and the crystalline (coherent) thickness, respectively, d denotes the lattice constant in the film.

$$A \propto \frac{\sin\left(\frac{\tilde{N} q_z d}{2}\right)}{\sin\left(\frac{q_z d}{2}\right)}, \tag{2}$$

where $\tilde{N}$ is the number of coherently scattering monolayers in the film. The distance between the minima of the associated oscillations in the intensity ($I=|A|^2$), ΔQ, is related to D^* by $D^*=\tilde{N}\times d=2\pi/\Delta Q$ [e.g., D^*_{DIP} and $\tilde{N}_{\mathrm{DIP}}$ are obtained from Figs. 5(a) and 6(a) with the known lattice constant $d_{\mathrm{DIP}}=16.56$ Å at room temperature].

(2) Rocking scans at a constant scattering angle $2\Theta=\alpha_i+\alpha_f$ at the position of Bragg reflections with varying angle of incidence, α_i, probe the angular distribution of the lattice planes, i.e., their mosaicity [full width at half maximum (FWHM) of the rocking curve, $\Delta\omega$].

(3) In "offset-scans," $\alpha_i=\alpha_f\pm\Delta\alpha$ is slightly offset from the specular condition and the diffusely scattered intensity is measured.

III. CHARACTERIZATION OF THE "AS-GROWN" STATE

The interfacial morphology of the samples immediately after deposition (as grown) has been characterized by cross-sectional TEM measurements as well as by x-ray measurements in the specular scan mode and in the offset scan mode with $\Delta\alpha=\pm 0.03°$, respectively. $\Delta\alpha$ is about twice the rocking width of the DIP(001) reflection ($0.013°$).[35]

The cross-sectional TEM images for samples A1–A4 as grown show large differences in the interfacial morphology depending on the preparation conditions (Fig. 3). The images suggest that the sample temperature during deposition has the predominant influence on the interface morphology.

Low temperature during Au deposition [Figs. 3(a) and 3(b)] leads to relatively well-defined interfaces with only a small amount of interdiffusion which is essentially independent of the deposition rate (R) in the range studied.

High-temperature Au deposition causes a much higher degree of interdiffusion into the DIP layer and a complex interfacial morphology. A high value of R leads to a fairly well-defined metal-organic interface [Fig. 3(c)], although the quality of this interface is lower than for the low-temperature samples (this will be discussed below). On the other hand, a low value of R in combination with high temperature results in complete intermixing of Au and DIP [Fig. 3(d)].

The morphological difference between "low-temperature samples" (A1, A2) and "high-temperature samples" (A3, A4) is also reflected in the specular (solid lines) and offspecular (dashed lines) x-ray data of Fig. 4:

The specular scans at the low-temperature samples A1 and A2 display Kiessig fringes with different periodicities associated with the thicknesses of both the Au and the DIP layer. This is evidence for rather homogeneous, smooth and well-defined films.

For the high-temperature samples, on the other hand (strongly damped), Kiessig fringes are visible only for sample A3. Furthermore, also the Kiessig fringes corresponding to the Au film in the offset scan are quickly damped out. For sample A4 Kiessig fringes are completely absent. These findings support the TEM observations of a rather rough and inhomogeneous interfacial morphology.

IV. ANNEALING PROCESS: DIP FILM

During the annealing studies, *in situ* x-ray measurements of the reflectivity as well as of the DIP(001) Bragg reflection were carried out.

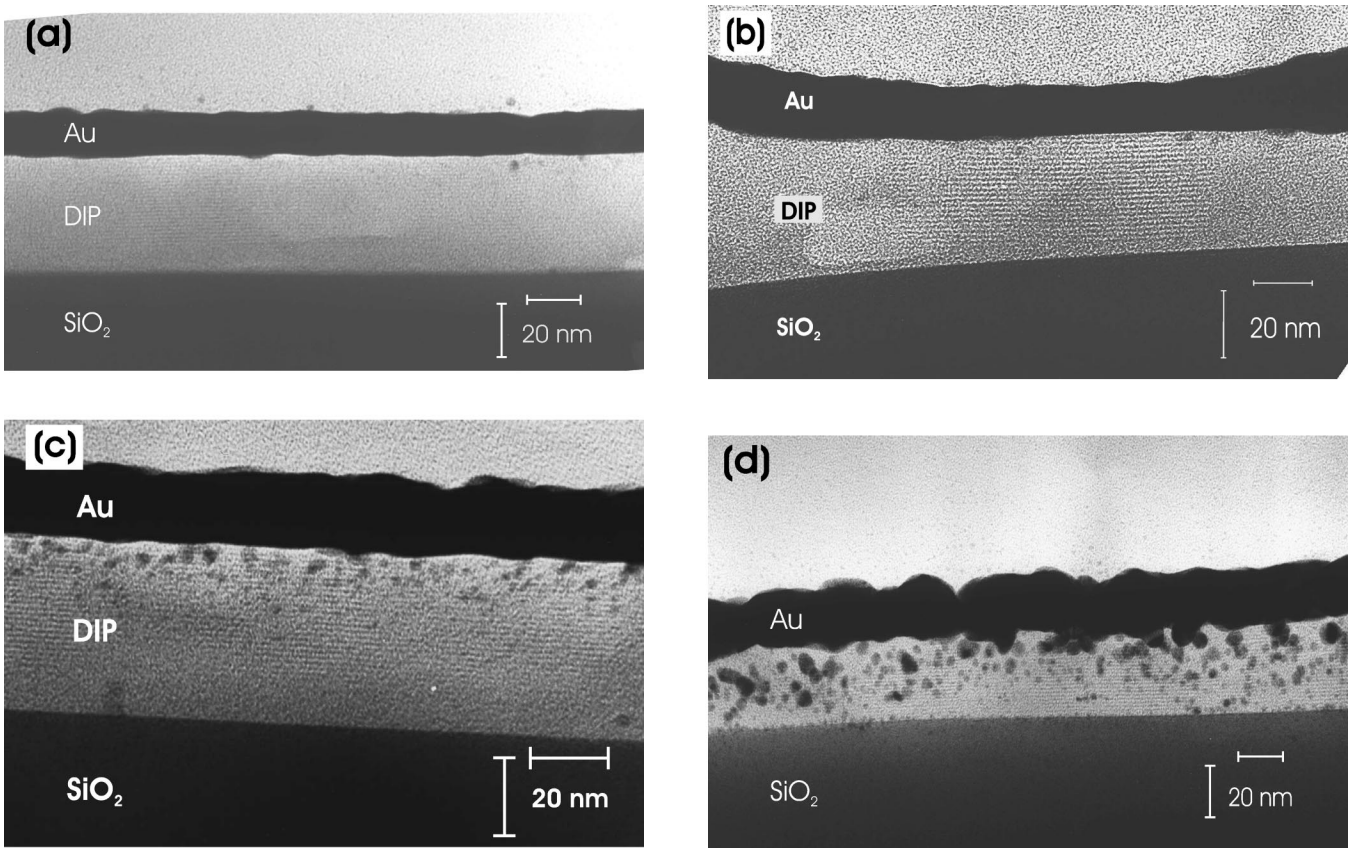

FIG. 3. Cross sectional TEM images of the samples (a) A1 ($T_{sub}=-120$ °C, $R=23$ Å/min), (b) A2 ($T_{sub}=-120$ °C, $R=0.35$ Å/min), (c) A3 ($T_{sub}=+70$ °C, $R=23$ Å/min), and (d) A4 ($T_{sub}=+70$ °C, $R=0.35$ Å/min).

A. Low-temperature samples ($T_{sub}=-120$ °C)

Figure 5(a) shows typical results of temperature dependent x-ray measurements as obtained for sample A2. Comparing D_{DIP} with D^*_{DIP} at room temperature after Au deposition shows that the DIP film is still ordered across its entire thickness since $D_{DIP}\approx D^*_{DIP}$. Almost undamped Laue oscillations are evidence for a high degree of lateral homogeneity of D^*_{DIP} in the DIP film.

Figure 5(b) shows N^*_{DIP} and D^*_{DIP} as a function of temperature for sample A2, which is typical for all investigated low-temperature samples.

Up to $T\approx 160$ °C N^*_{DIP} is essentially stable. This implies a high degree of thermal stability of the DIP layer and is the same temperature as for uncapped DIP films.[36] The coherent thickness D^*_{DIP} remains essentially constant (increase by ≈ 1 ML, i.e., $\approx 5\%$), while the intensity increases by $\approx 20\%$ for sample A2 (and by $\approx 40\%$ for sample A1). The latter observation is indicative of a reordering process in the DIP film, which takes place at elevated temperatures.

For $T\geqslant 160$ °C destruction of the DIP layer by thermal desorption of molecules is evidenced by a pronounced decrease of N^*_{DIP} while D^*_{DIP} remains stable.

B. High-temperature samples ($T_{sub}=+70$ °C)

Figure 6(a) shows typical temperature dependent specular x-ray measurements as obtained for sample A3. Similar to the low-temperature samples, we find $D_{DIP}\approx D^*_{DIP}$, and thus the DIP film is still coherently ordered across its entire thickness after Au deposition.[37] However, the Laue oscillations around the DIP(001) Bragg reflection are considerably damped, indicative of D^*_{DIP} being laterally rather inhomogeneous. It is plausible to attribute this observation to the interdiffusion of considerable amounts of Au into the DIP film during deposition which leads to destruction of parts (A3) or large areas (A4) of the DIP film as was also observed in the TEM images [Figs. 3(c) and 3(d)].

Figure 6(b) shows N^*_{DIP} and D^*_{DIP} associated with sample A3 as a function of annealing temperature; it is representative for all high-temperature samples in our study.

Obviously, in the high-temperature samples, the DIP film exhibits essentially the same thermal stability ($T\approx 150$ °C) as the low-temperature samples.[38] However, in contrast to the low-temperature samples, at temperatures below the onset of desorption the intensity of the DIP(001) reflection remains essentially constant within the experimental error. Thus, no indication of a reordering process in the DIP layer is observed for the high-temperature samples.

For still higher temperatures ($T\geqslant 160$ °C), destruction of the DIP layer in samples A3 and A4 is evidenced by a pronounced decrease of N^*_{DIP} while D^*_{DIP} remains stable.

V. ANNEALING PROCESS: AU FILM

To characterize the crystalline state of the Au layer on top of the DIP film the Au(111) reflection was used allowing

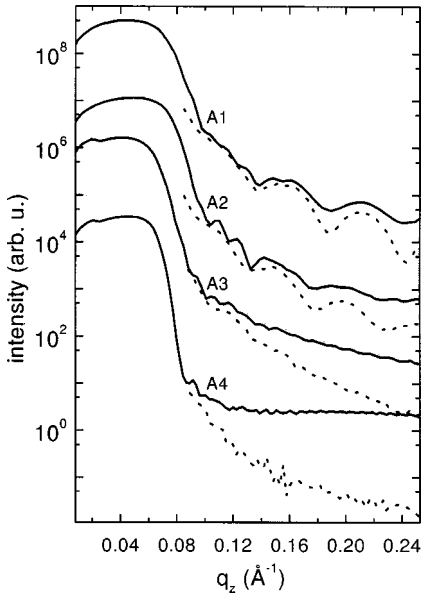

FIG. 4. Specular and offset scans for each of the four samples A1–A4. In each set of data the solid curve corresponds to the specularly reflected intensity, containing the intensity of both the DIP and the Au layers. The dotted curves on the other hand were recorded with the sample slightly offset from the specular condition ($\Delta\alpha = +0.03°$). The individual data sets are shifted with respect to each other for the sake of clarity.

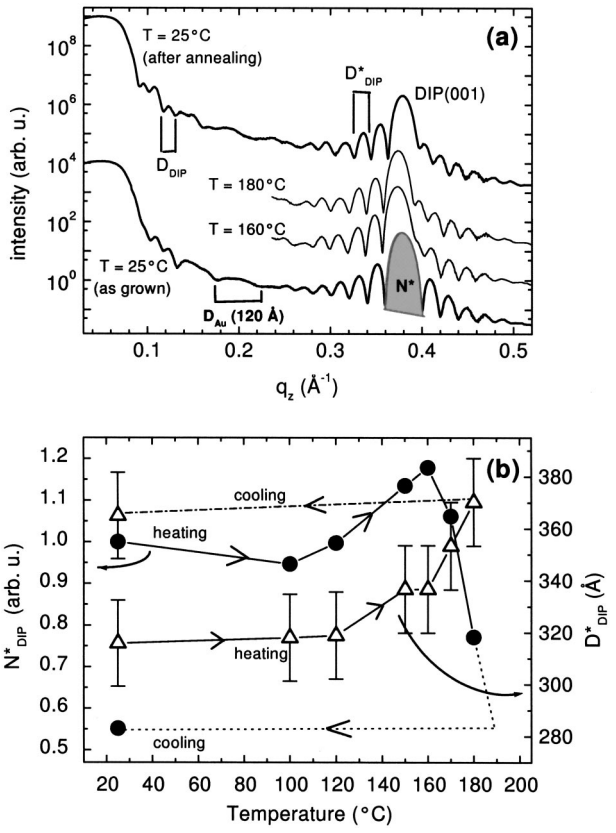

FIG. 5. (a) Specular scan over the DIP(001) Bragg reflection at various temperatures for a typical low-temperature sample, A2. (b) N^*_{DIP} (●) [shaded area in (a)] and D^*_{DIP} (△) of sample A2 as a function of the annealing temperature.

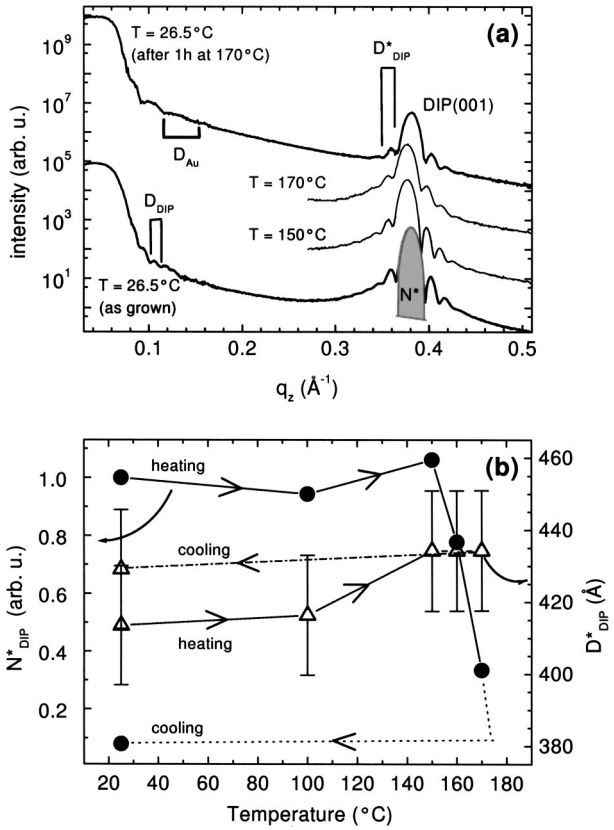

FIG. 6. (a) Specular scan over the DIP(001) Bragg reflection at various temperatures for a typical high-temperature sample, A3. (b) N^*_{DIP} [●, shaded area in (a)] and D^*_{DIP} (△) of sample A3 as a function of the annealing temperature.

for the determination of the crystalline orientation of the grains in the Au film with respect to the surface normal. The coherent thickness of the Au grains, D^*_{Au} was obtained by analyzing the specular width of the Au(111) reflection and its Laue oscillations [see Fig. 2 and Eq. (2)]. The integrated intensity of the Au(111) reflection is related to the total number of Au atoms, N^*_{Au}, which exhibit (111) orientation. From rocking scans across the Au(111) Bragg reflection, the mosaicity ($\Delta\omega$) of the Au grains with (111) orientation along the surface normal is deduced (see Fig. 2).

A. Low-temperature samples ($T_{\mathrm{sub}} = -120$ °C)

Figure 7(a) shows a typical set of specular scans over the Au(111) reflection as grown and after the annealing procedure, respectively. Figure 7(b) displays the typical evolution of N^*_{Au} and of $\Delta\omega$ as a function of temperature for the low-temperature samples. In the as-grown state, N^*_{Au} is fairly low. We note that N^*_{Au} of the as-grown state is essentially the same for all investigated low-temperature samples. At the same time, the mosaicity of the Au grains is relatively high ($\Delta\omega \approx 10°$, centered around the surface normal). Nevertheless, given that in this system Au is evaporated onto an organic film it is remarkable that obviously a strong (111) texture forms.

Up to $T = 100$ °C the mosaicity as well as N^*_{Au} remain almost constant. Further increasing the temperature results

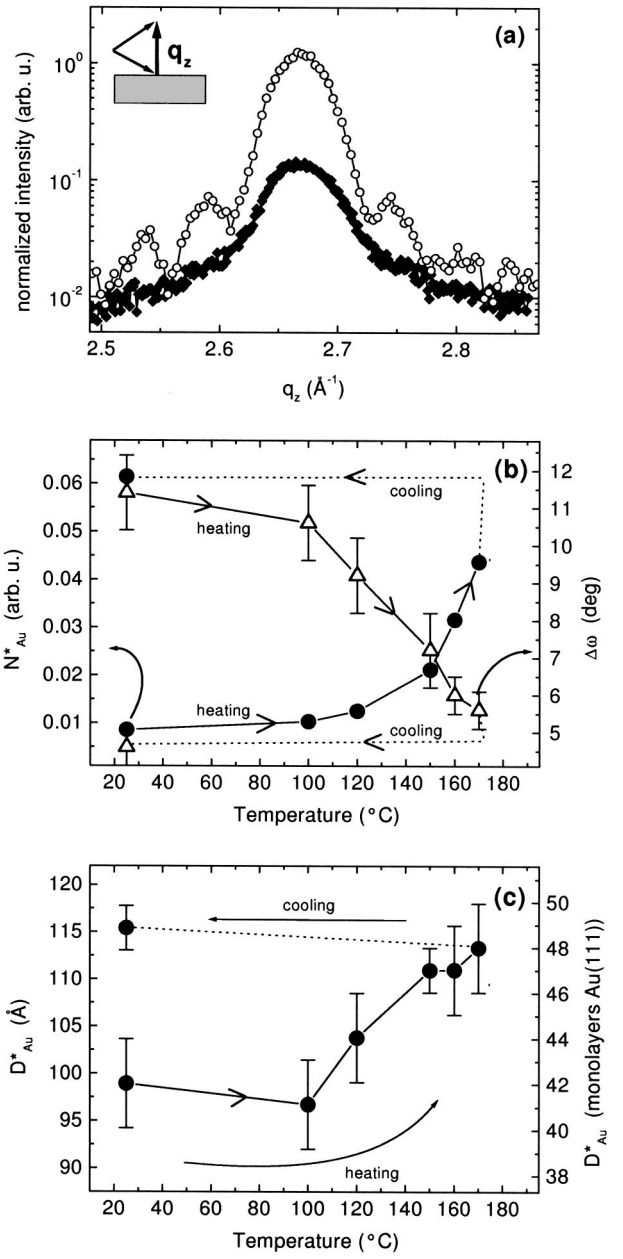

FIG. 7. (a) Specular scan through the Au(111) Bragg reflection of sample A1 as grown (♦) and after the annealing procedure (○). The inset displays the scattering geometry used for these scans. (b) N^*_{Au} (●, left axis) and $\Delta\omega$ of the Au(111) reflection, i.e., mosaicity, (△, right axis) for sample A1. (c) D^*_{Au} of the Au(111) grains in the Au film of A1. D^*_{Au} is given in Å for the left axis and in monolayers at the right axis.

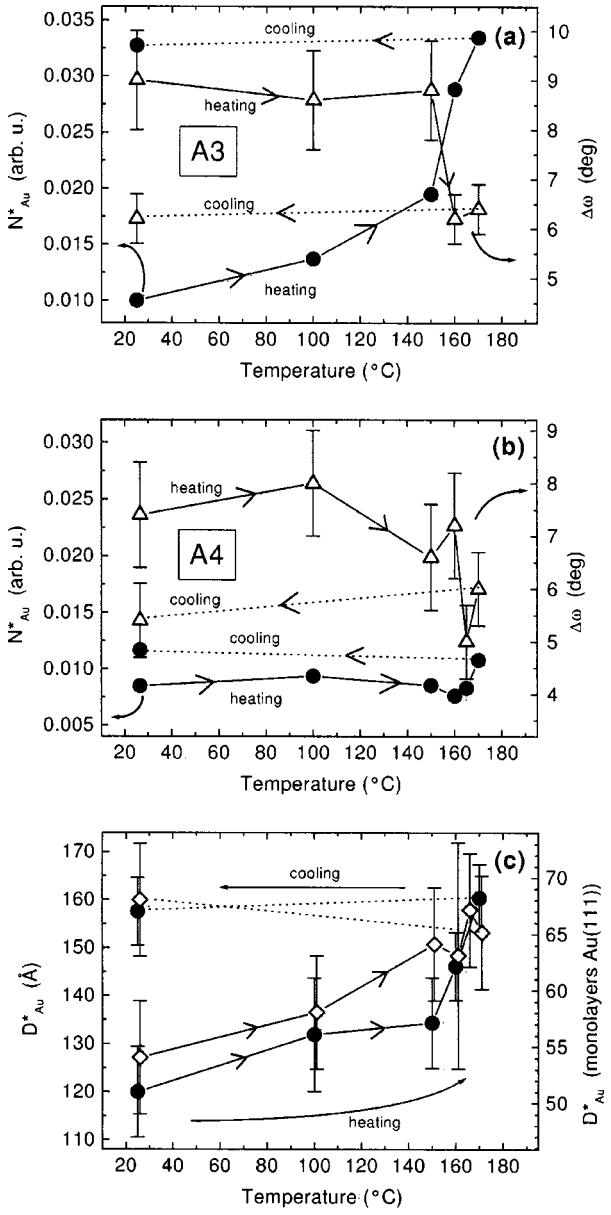

FIG. 8. N^*_{Au} (●, left axis) and $\Delta\omega$ of the Au(111) reflection, i.e., mosaicity, (△, right axis) for (a) sample A3, and (b) sample A4. (c) D^*_{Au} of the Au(111) grains in the Au film of A3 (●) and A4 (red ◇). D^*_{Au} is given in Å for the left axis and in monolayers at the right axis.

initially in a pronounced decrease of the mosaicity, while N^*_{Au} increases.

Figure 7(c) shows the typical evolution of D^*_{Au} as a function of temperature for the low-temperature samples. The decrease of the specular peak width is related to an increase in coherent thickness of ≈20% during the annealing. Moreover, the appearance of Laue oscillations for $T \gtrsim 120$ °C is evidence for the existence of ordered Au grains [(111) orientation], which exhibit a quite homogeneous thickness in the sample.

Combining the observations of an increase in N^*_{Au}, a decrease of the Au(111) mosaicity and an increase in the coherent thickness of Au grains with (111) orientation suggests a pronounced reordering process in the Au layer for $T \geqslant 120$ °C. This process leads to a preferential (111) orientation of the grains in the film along the *z* axis, which usually is the energetically favored orientation for thin Au films. Additional evidence for this interpretation is given by the continuously decreasing intensity of the Au(200) reflection [noncollinear with the Au(111) reflection] along the surface normal which has also been recorded during the annealing.

B. High-temperature samples ($T_{sub} = +70$ °C)

Figures 8(a) and 8(b) display the evolution of N^*_{Au} and of $\Delta\omega$ as a function of temperature for samples A3 and A4, respectively.

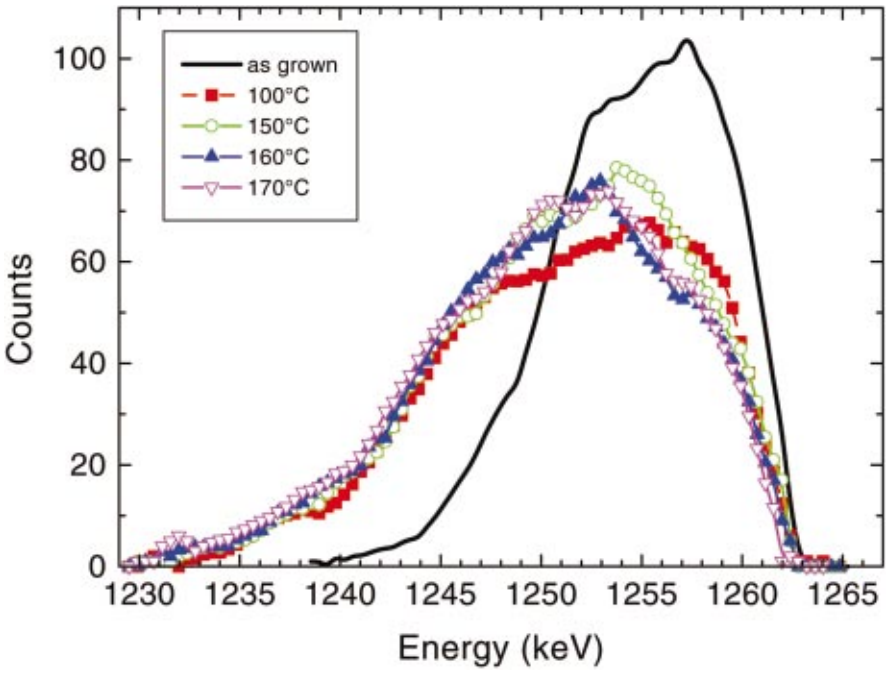

FIG. 9. (Color) RBS measurements around the Au edge of sample A5. The figure shows the spline-fitted RBS Au peak just after Au deposition (black solid line), and after annealing at $T = 100\,^{\circ}\mathrm{C}$ (red ■), 150 °C (green ○), 160 °C (blue ▲), and 170 °C (magenta ▽) for 1 h each.

For both samples, N^*_{Au} in the as-grown state is essentially the same as for A1 and A2. However, N^*_{Au} increases only by a factor of 3.5 (compared to a factor of 7 and 12 for the low temperature samples A1 and A2, respectively) during the annealing while $\Delta\omega$ remains constant up to $T = 150\,^{\circ}\mathrm{C}$.

Figure 8(c) shows D^*_{Au} as a function of annealing temperature for samples A3 and A4. For both samples, D^*_{Au} exhibits a pronounced increase of $\approx 30\%$ for $T > 150\,^{\circ}\mathrm{C}$. However, Laue oscillations appear only after annealing at the highest temperature and are rather smeared out. This implies that the grains inside the film exhibit a fairly broad distribution of coherent thicknesses, in contrast to the observations at the low-temperature samples. In conclusion, the annealing behavior of sample A3 resembles that of the low-temperature samples, although there remain differences with regard to the crystalline homogeneity of the Au layer.

The structural behavior of the Au layer of sample A4 upon annealing is not comparable to any of the other samples, consistent with the highly intermixed structure of this heterosystem.

VI. ANNEALING PROCESS: AU/DIP INTERFACE

In a previous communication,[22] we have shown that for Au films with a thickness of 70 Å (exceeding the roughness of the pristine DIP film by a factor of 2) the Au/DIP interface is thermally stable at least up to 100 °C on a time scale of 1 h. For larger temperatures, first, interdiffusion of Au into the DIP film has been observed, followed, at still higher temperatures ($T > 150\,^{\circ}\mathrm{C}$), by the evolution of a closed layer of material (presumably DIP) on top of the Au film.

Here, we have further investigated the thermal stability of the Au/DIP interface for a Au film with a nominal thickness of 35 Å, which now is of the order of the surface roughness of the pristine DIP film (see Ref. 28).

In situ temperature-dependent high-energy resolution RBS measurements were carried out using sample A5. In Fig. 9 the smoothened RBS Au peak is displayed. It has been recorded just after deposition and after 1 h annealing at each temperature indicated in Fig. 9. Immediately after deposition, the Au peak exhibits a slightly smeared-out shape with relatively steep edges at the high and low-energy side indicative of an essentially homogeneous and well-defined film with only little interdiffusion (similar to samples A1 and A2, although the deposition conditions for the Au film were, for technical reasons, somewhat different from these samples; see Table I).

Annealing the sample at 100 °C for 1 h already results in a marked interdiffusion of Au into the DIP film visible in the change of the shape of the peak. We note that the smearing of the Au edge may also be due to a certain degree of diffusion of DIP molecules onto the Au film. However, closer inspection of the peak shows that the Au edge at this temperature is still at the same position, i.e., there is still Au at the surface uncovered by DIP. Comparison with the 70 Å film [no change of the shape visible at 100 °C (Ref. 22)] suggests that Au interdiffusion into the DIP film is the major contribution to the change of the peak shape for the present sample. The maximum peak height decreases by $\approx 20\%$, indicating that the area of the sample covered with Au has decreased. This may be viewed as a dewetting process of the Au- layer.

Further annealing to higher temperatures shows that the diffusion process of the Au into the DIP has essentially been completed at 100 °C. Nevertheless, at the two highest annealing temperatures, the position of the Au edge shifts to lower energies by ≈ 1 keV. This implies that the complete Au film at these temperatures is covered by a thin film (presumably DIP) of about 15 Å in thickness which was also observed for the thick Au film of Ref. 22.

Note that for the 70 Å Au film the final state of Au interdiffusion has been observed for $100\,^{\circ}\mathrm{C} < T \leqslant 150\,^{\circ}\mathrm{C}$. This suggests that the temperature at which enhanced Au diffusion sets in depends on the Au thickness. Presumably,

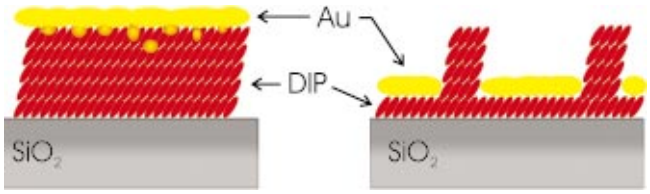

FIG. 10. (Color) Model for the desorption process of the DIP in a system of Au/DIP. On the left side the system is shown prior to the annealing process. The image on the right-hand side depicts the situation during and after the annealing process in which some DIP islands remain unchanged in thickness.

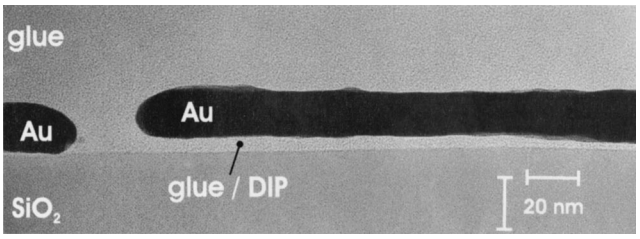

FIG. 11. Cross-sectional TEM micrograph showing a sample prepared similar to A1. The sample has been annealed at $T=170\,^{\circ}\mathrm{C}$ until only 5% of the DIP(001) Bragg-reflection intensity remained (see Ref. 22). The Au layer is separated from the SiO_2 substrate only by a small organic layer. The Au film exhibits holes with curved edges where presumably DIP islands resisted the thermal treatment.

due to the formation of immobile Au clusters, the Au diffusion stops after only a short time interval.

VII. DISCUSSION

TEM images as well as specular and off-specular x-ray measurements show that the interfacial morphology is critically dependent on the conditions during Au deposition. Low sample temperatures ($-120\,^{\circ}\mathrm{C}$) lead to Au layers of rather homogeneous thickness and quite well-defined interfaces although a small amount of Au interdiffusion into the organic layer seems to be unavoidable without a ''reactive'' diffusion barrier at the metal–organic interface. In contrast to the interfacial morphology between Au and DIP, the average crystalline orientation of the Au grains in the cap layer appears to be largely unaffected by the substrate temperature during deposition in the temperature interval studied. Comparing N^{*}_{Au} and $\Delta\omega_{\mathrm{Au}}$ shows that these quantities are nearly the same for all investigated samples. Thus, the formation of grains in the Au film is essentially independent of the substrate temperature and of the deposition rate in the range of rate and temperature investigated.

Combining the results of x-ray scattering, RBS, and TEM measurements, the following scenario for the changes in the heterostructure upon annealing is proposed (see also Fig. 10).

For sufficiently thick Au films [$\geqslant 70$ Å (Ref. 22)], the heterosystem is thermally stable up to $T\approx 100\,^{\circ}\mathrm{C}$ on a time scale of 1 h (left-hand side of Fig. 10).

For $100\,^{\circ}\mathrm{C}<T\lesssim 150\,^{\circ}\mathrm{C}$, interdiffusion of Au into the DIP film is promoted. This may support the reordering process in the Au film indicated by a decreasing $\Delta\omega$ of grains with Au(111) orientation parallel to the surface normal and a slight increase of N^{*}_{Au}. In addition, a reordering process in the DIP film is observed (increasing N^{*}_{DIP}). Nevertheless, at this point, the DIP film as such and, presumably, the interface remain essentially stable. The fact that the RBS Au edge does not shift to lower energies at these temperatures suggests that the diffusion of DIP molecules onto the Au layer is only of minor importance even for the smearing of the RBS Au edge of the 35 Å Au film.

At still higher temperatures ($T\gtrsim 155\,^{\circ}\mathrm{C}$) the DIP film becomes thermally unstable.[38] DIP molecules start to diffuse onto the Au film where they form a closed layer (shift of the RBS Au edge to lower energies) and desorb (decrease of N^{*}_{DIP}). In addition, enhanced Au interdiffusion sets in,[22] accompanied by a pronounced reorientation of the Au film as well as by increasing D^{*}_{Au}.

The x-ray data suggest that the destruction of the DIP film is accomplished by a laterally inhomogeneous desorption process: the DIP film splits into laterally separated islands of homogeneous thickness (constant D^{*}_{DIP} and $\Delta\omega_{\mathrm{DIP}}$, but decreasing N^{*}_{DIP}). This scenario is supported by Fig. 11. It shows a cross-sectional image of a sample prepared equivalent to A1 which has been annealed at $T=170\,^{\circ}\mathrm{C}$ until $\approx 95\%$ of the DIP film has been destructed by desorption. The DIP islands are separated by areas which are presumably filled with Au (see sketch on the right hand side of Fig. 10). An electronic device using DIP as organic semiconductor will break down due to the islanding effect or at the latest from the onset of DIP desorption.

It must be pointed out that the finding of a *laterally inhomogeneous* desorption process of the DIP film in the heterosystem is in contrast to the observation of a *laterally homogeneous* desorption process for uncapped DIP films which was found previously.[36] Apparently, the presence of a Au film (with $D\geqslant 70$ Å) has a strong influence on the desorption behavior of the DIP film. It is plausible to assume that stacks of DIP covered by a *closed* Au layer resist to a higher temperature than stacks of DIP, which are uncapped or whose molecules can diffuse through cracks in the cap layer. Thus, in this picture, the Au layer induces a complete change in the desorption process of the DIP layer.

RBS measurements showed that Au layers with a larger thickness ($\gtrsim 70$ Å) exhibit a greater thermal stability of $T\approx 100\,^{\circ}\mathrm{C}$ of the Au/DIP interface against Au interdiffusion into the DIP film[22] than samples with thinner Au films. A possible interpretation is that for Au films with a thickness of the order of the surface roughness of the organic film ($\sigma\approx 25$ Å for our samples[28]) the sample might exhibit a larger fraction of areas where the Au film is not closed and thus small isolated Au clusters are present. These are expected to be fairly mobile and may easily diffuse into the organic layer at elevated temperatures. On the other hand, in a ''thick'' Au layer, most of the Au atoms may be considered as being coalesced in large Au clusters which are essentially immobile even at elevated temperatures. After the organic layer itself starts to deteriorate, interdiffusion is facilitated.

VIII. SUMMARY AND CONCLUSIONS

In conclusion, it was shown that the interfacial properties of metal contacts on organic materials in the system Au on DIP are strongly determined by the preparation conditions of the Au film. Moreover, it was found that the interface is essentially stable against further interdiffusion up to 100 °C if the Au film exhibits a sufficient thickness ($\geqslant 70$ Å). These findings are relevant for device fabrication. If no ''reactive'' diffusion barrier between the metal and the functional organic layer is employed, the diffusion may be ''frozen in'' by the proper choice of the deposition conditions. Au thicknesses large compared to the surface roughness of the organic material at low substrate temperatures during deposition (-120 °C) lead to rather well-defined interfaces which exhibit a thermal stability sufficient for typical technical applications.

In addition, it could be demonstrated that the Au film of the low-temperature samples undergoes a reordering process for $T \gtrsim 120$ °C. This is accompanied by pronounced reorientation of the Au grains for $T \geqslant 150$ °C, which leads to a preferential orientation of the Au grains with Au(111) orientation parallel to the surface normal.

Further, it was shown, that the DIP structure in the Au/DIP heterosystem is thermally stable up to 150 °C and that the DIP film in the heterosystem exhibits a laterally inhomogeneous desorption process for $T \geqslant 160$ °C, which is related to the Au film. This desorption process is qualitatively different from the laterally homogeneous desorption observed for uncapped DIP films.

ACKNOWLEDGMENTS

The authors wish to thank S. Sellner, O. Osso, and H. Bender for help during the experiments; V. Sharma for help in the data analysis; and N. Karl for useful discussions. One of the authors (F.S.) acknowledges support from the DFG within the focus program ''Organische Feldeffekt-Transistoren.''

[1] S. R. Forrest, Chem. Rev. **97**, 1793 (1997).
[2] J. Kalinowski, J. Phys. D **32**, R179 (1999).
[3] W. E. Howard and O. F. Prache, IBM J. Res. Dev. **45**, 115 (2001).
[4] J. S. Wilson, A. S. Dhoot, A. J. A. B. Seeley, M. S. Khan, A. Köhler, and R. H. Friend, Nature (London) **413**, 828 (2001).
[5] S. E. Shaheen, R. Radspinner, N. Peyghambarian, and G. E. Jabbour, Appl. Phys. Lett. **79**, 2996 (2001).
[6] E. A. Katz, D. Faiman, S. M. Tuladhar, J. M. Kroon, M. M. Wienk, T. Fromherz, F. Padinger, C. J. Brabec, and N. S. Sariciftci, J. Appl. Phys. **90**, 5243 (2001).
[7] Ch. D. Dimitrakopoulos and P. R. L. Malenfant, Adv. Mater. **14**, 99 (2002).
[8] B. Crone, A. Dodabalpur, Y.-Y. Lin, R. W. Filas, Z. Bao, A. Laduca, R. Sarpeshkar, H. E. Katz, and W. Li, Nature (London) **403**, 521 (2000).
[9] G. H. Gelinck, T. C. T. Geuns, and D. M. de Leeuw, Appl. Phys. Lett. **77**, 1487 (2000).
[10] B. Crone, A. Dodabalapur, A. Gelperin, L. Torsi, H. Katz, A. J. Lovinger, and Z. Bao, Appl. Phys. Lett. **78**, 2229 (2001).
[11] F. Faupel, R. Willecke, and A. Thran, Mater. Sci. Eng., R. **22**, 1 (1998).
[12] D. Gupta, F. Faupel, and R. Willecke, in *Diffusion in Amorphous Materials* (The Minerals, Metals and Materials Society, Pittsburgh, PA, 1994).
[13] R. Tromp, F. LeGoues, and P. Ho, J. Vac. Sci. Technol. A **3**, 782 (1985).
[14] R. Weber, K.-M. Zimmermann, M. Tolan, J. Stettner, W. Press, O. H. Seeck, J. Erichsen, V. Zaporojtchenko, T. Strunskus, and F. Faupel, Phys. Rev. E **64**, 061508 (2001).
[15] D.-Q. Yang and E. Sacher, J. Appl. Phys. **90**, 4768 (2001).
[16] D.-Q. Yang and E. Sacher, J. Phys.: Condens. Matter **14**, 7097 (2002).
[17] G. Philipp, C. Müller-Schwanneke, M. Burghard, S. Roth, and K. v. Klitzing, J. Appl. Phys. **85**, 3374 (1999).
[18] Y. Hirose, A. Kahn, V. Aristov, P. Soukiassian, V. Bulovic, and S. R. Forrest, Phys. Rev. B **54**, 13748 (1996).
[19] C. Shen and A. Kahn, J. Appl. Phys. **90**, 4549 (2001).
[20] C. Shen, A. Kahn, and J. Schwartz, J. Appl. Phys. **90**, 6236 (2001).
[21] C. Parthasarathy, C. Shen, A. Kahn, and S. R. Forrest, J. Appl. Phys. **89**, 4986 (2001).
[22] A. C. Dürr, F. Schreiber, M. Kelsch, H. D. Carstanjen, and H. Dosch, Adv. Mater. **14**, 961 (2002).
[23] K. A. Ritley, K.-P. Just, F. Schreiber, H. Dosch, T. P. Niesen, and F. Aldinger, J. Mater. Res. **15**, 2706 (2000).
[24] A. C. Dürr, F. Schreiber, M. Münch, N. Karl, B. Krause, V. Kruppa, and H. Dosch, Appl. Phys. Lett. **81**, 2276 (2002).
[25] N. Karl in *Charge Carrier Mobility in Organic Crystals, Organic Electronic Materials*, edited by R. Farchioni and G. Grosso (Springer, Berlin, 2001), p. 283.
[26] B. D. Silverman, Macromolecules **24**, 2467 (1991).
[27] P. Jensen, Rev. Mod. Phys. **71**, 1695 (1999).
[28] A. C. Dürr, F. Schreiber, K. A. Ritley, V. Kruppa, J. Krug, H. Dosch, and B. Struth, Phys. Rev. Lett. **90**, 016104 (2003).
[29] A. C. Dürr, F. Schreiber, M. Kelsch, and H. Dosch, Ultramicroscopy (in print 2003).
[30] H. D. Carstanjen, W. Decker, and H. Stoll, Z. Metallkd. **84**, 368 (1993).
[31] T. Enders, M. Rilli, and H. D. Carstanjen, Nucl. Instrum. Methods Phys. Res. B **64**, 817 (1992).
[32] The temperature of $T = 180$ °C (samples A1 and A2) was applied for ≈ 15 min only; this was the period in which the x-ray reflectivity and the specular DIP(001) reflection were measured. After a significant decrease in intensity at the DIP(001) reflection was noticed, the temperature was set back to room temperature.
[33] M. Tolan, *X-Ray Scattering from Soft-Matter Thin Films* (Springer, Berlin, 1999).
[34] In our study: Au atoms or DIP molecules.
[35] I. D. Kaendler, O. H. Seeck, J.-P. Schlomka, M. Tolan, W. Press, J. Stettner, L. Kappius, C. Dieker, and S. Mantl, J. Appl. Phys. **87**, 133 (2000).
[36] A. C. Dürr, Ph.D. thesis, Stuttgart University (2002); http://elib.uni-stuttgart.de/opus/volltexte/2002/1215/
[37] Sample A4 does not exhibit Kiessig fringes. Thus, the evaluation of the DIP- film thickness was made based on the values determined during the DIP deposition by the quartz-crystal microbalance and from the thickness observed in the TEM image of the film, respectively.
[38] Samples A1 and A2 have been investigated in a different Synchrotron run than samples A3 and A4. We attribute the observed differences in thermal stability of the DIP layer between samples A1 and A2 on the one hand and A3 and A4 on the other hand to slight differences in the experimental setup (efficiency of the heating; thermal coupling, etc.).